Differential Stereocontrolled Formation of Tricyclic Triterpenes by Mutation of Tyrosine 99 of the Oxidosqualene-Lanosterol Cyclase from *Saccharomyces cerevisiae*

Tung-Kung Wu,*[a] Wen-Hsuan Li,[a] Cheng-Hsiang Chang,[a] Hao-Yu Wen,[a] Yuan-Ting Liu,[a] and Yi-Chun Chang[a]

The function of the Tyr99 residue from *Saccharomyces cerevisiae* oxidosqualene-lanosterol cyclase (ERG7) was analyzed by constructing deletion and site-saturated mutants. Two truncated intermediates, (13αH)-isomalabarica-14Z,17E,21-trien-3β-ol and (13αH)-isomalabarica-14E,17E,21-trien-3β-ol, were isolated from the ERG7^{Y99X} mutants. These results suggest that the functional role of ERG7^{Y99} is to affect both chair–boat 6–6–5 tricyclic Markovnikov C-14 cation stabilization and the stereochemistry of the protons at the C-15 position for subsequent deprotonation.

(© Wiley-VCH Verlag GmbH & Co. KGaA, 69451 Weinheim, Germany, 2009)

Introduction

Oxidosqualene-lanosterol cyclases catalyze the conversion of (3S)-2,3-oxidosqualene (OS, **1**) to lanosterol (LA, **2**). The same substrate is utilized to synthesize cycloartenol by oxidosqualene-cycloartenol synthase. An intricate and yet highly stereo- and regiospecific cationic cyclization/rearrangement mechanism that encompasses substrate conformational prefolding, oxirane ring protonation and cleavage, cation/π interaction-directed consecutive tetracyclic ring annulation, 1,2-shifted hydride and methyl group migration, and final specific deprotonation, has been proposed for both enzymes.[1,2] Recently, the elucidation of the complexities of the oxidosqualene cyclases, including the catalytic mechanism, functional role of specific amino acid residues, and mutation-induced product specificity/diversity profile, has been greatly facilitated through substrate analogues, site-specific mutagenesis coupled with product characterization, and X-ray crystallographic analyses.[3–20] However, the important residues involved in stereo- or regiospecific control of these product profiles remain unclear.

The catalytic importance of the Tyr98 residue of human oxidosqualene-lanosterol cyclase (OSC) was inconspicuous until the recent X-ray crystallographic analysis of the protein structure.[13] Homology modeling between bacterial squalene-hopene cyclase and human OSC showed that a one-residue insertion above and a one-residue deletion below the molecular plane of the substrate were observed in the human OSC enzyme.[21] Additionally, the Tyr98 of the human OSC was thought to be spatially positioned to enforce the energetically unfavorable boat conformation of OS for lanosterol B-ring formation by pushing the methyl group at C-8 (lanosterol numbering) below the molecular plane.[13] The Tyr99 residue of *Saccharomyces cerevisiae* oxidosqualene-lanosterol cyclase (ERG7) corresponds to the Tyr98 residue in human OSC. *S. cerevisiae* ERG7 has 40% sequence identity and 55% similarity with human OSC. We previously performed site-saturated mutagenesis experiments on the Trp232, His234, Phe445, Tyr510, and Tyr707 residues of ERG7 to determine their catalytic activities and product profiles.[11,14–17,19] The results showed that both the ERG7^{F445X} and ERG7^{H234X} mutant enzymes produced truncated tricyclic and altered deprotonation products, indicating the catalytic role of the residues in cationic stabilization at the C-14 position for the tricyclic product, and/or the C-8/C-9 position for the final deprotonation product. In addition, a π-electron-rich pocket of aromatic residues around the Phe445 residue of ERG7 was suggested to either stabilize the electron-deficient cationic intermediate or to be responsible for the equilibrium shift toward the lanosteryl C-8/C-9 cation during the rearrangement process and for the formation of lanosterol. Of those aromatic residues, Tyr99 was located at a distance of approximately 3.7 Å, within range to interact with the Phe445 residue, and close to the C/D ring of the substrate.[16] In addition, although alignment of multiple sequences revealed that the Tyr99 residue of ERG7 is highly conserved in both oxidosqualene-lanosterol cyclases and oxidosqualene-cycloartenol synthases, different amino acids were at that position in related enzymes β-amyrin synthase and lupeol synthase. Also, a

[a] Department of Biological Science and Technology, National Chiao Tung University,
300 Hsin-Chu, Taiwan, Republic of China
Fax: +886-3-5725700
E-mail: tkwmll@mail.nctu.edu.tw

Supporting information for this article is available on the WWW under http://dx.doi.org/10.1002/ejoc.200900638.

one-residue insertion proximal to the Tyr99 position of ERG7 was observed in oxidosqualene-lanosterol cyclases from *S. cerevisiae*, *Trypanosoma brucei*, and *T. cruzi*, but not in mammalian oxidosqualene-lanosterol cyclases (data not shown). The combination of these observations suggested that Tyr99 of *S. cerevisiae* ERG7 may have a different functional role than Tyr98 in human OSC. However, no mutation-induced product isolation and characterization were performed to validate the above-mentioned hypothesis about the catalytic mechanism.

To further substantiate the functional role of the Tyr99 position in the ERG7-catalyzed cyclization/rearrangement cascade and to investigate the effects of substitutions of other amino acid residues on the catalytic activity and product profile of the cyclase, we generated a mutant ERG7 on which the Tyr99 residue was deleted (ERG7$^{\Delta Y99}$) and a set of mutants carrying every amino acid substitution at that position (site-saturated mutations, ERG7^{Y99X}) and characterized products profiles. Two abortive cyclization products, (13α*H*)-isomalabarica-14Z,17E,21-trien-3β-ol (**3**) and (13α*H*)-isomalabarica-14E,17E,21-trien-3β-ol (**4**), were isolated, for the first time, from several mutants expressing ERG7^{Y99X} as the sole oxidosqualene cyclase. In addition, compounds **3** and **4** were isolated concomitantly from the ERG7^{Y99X} mutants that produced truncated products, but at different ratios. These product profiles correspond to truncation of the cyclization/rearrangement cascade at the chair–boat 6–6–5 tricyclic Markovnikov cation, at the C-14 position, and subsequent abstraction of protons at the C-15 position with different stereochemical preferences. A similar truncated intermediate, (13α*H*)-isomalabarica-14(26),17E,21-trien-3β-ol (**5**), which is derived from the same C-14 position that directly abstracts the C-26 proton, was previously isolated from both ERG7^{F445X} and the ERG7^{H234X} mutants.[15,16] Conversely, compound **5** could not be isolated from any of the ERG7^{Y99X} mutants. These results suggested a catalytic role of the Tyr99 residue in ERG7 that not only stabilizes the same chair–boat 6–6–5 tricyclic Markovnikov cation as that of Phe445 and His234, but also affects different deprotonation positions, perhaps through different spatial orientations or interactions with other proximal residues within the active site cavity.

Results and Discussion

We generated the ERG7$^{\Delta Y99}$ and ERG7^{Y99X} mutations by using the QuikChange site-directed mutagenesis kit.[15,17] Following the confirmation of the amino acid substitutions at the Tyr99 position, the recombinant plasmids were transformed into yeast HEM1 ERG7 double-knockout mutant TKW14, which is only viable when complemented with cyclase activity derived from ERG7^{Y99X} or when supplied with exogenous ergosterol. The TKW14[pERG7^{Y99X}] strain expressed ERG7^{Y99X} as the only oxidosqualene cyclase. The genetic selection results showed that all mutations at Tyr99 supported ergosterol-independent growth of TKW14, except for the Tyr99 deletion and the Tyr99Asn and Tyr99His

mutations. These results indicated a functional role for Tyr99 in catalysis or structure stabilization. Next, the product profiles of each mutant were characterized by growing the mutant strains, preparing the nonsaponifiable lipid extract (NSL), separating the fractions on a AgNO$_3$-impregnated silica gel column, and analyzing the structures of each product by using gas chromatography–mass spectrometry (GC–MS) and nuclear magnetic resonance (^{1}H, ^{13}C NMR, DEPT, ^{1}H–^{1}H COSY, HMQC, HMBC, and NOE).

Product profiles of the ERG7$^{\Delta Y99}$ and ERG7^{Y99X} mutants are summarized in Table 1. No products with molecular masses of $m/z = 426$ were observed for the nonviable mutants, consistent with the genetic results. The viable mutants produced either lanosterol alone or lanosterol and two unidentified compounds with a C$_{30}$H$_{50}$O formula. The first new compound was identified by NMR spectroscopy as (13α*H*)-isomalabarica-14Z,17E,21-trien-3β-ol (**3**), a chair–boat (C–B) 6–6–5 tricyclic product with *trans–syn–trans* stereochemistry and $\Delta^{14Z,17E,21}$ double bonds. Confirmation of the structure, including both the bond connectivity and stereochemistry, is described in the Experimental Section. Specifically, the presence of NOE interactions among 3-H/Me-29, Me-30/Me-28, Me-29/5-H, 3-H/5-H, Me-28/9-H, 15-H/Me-26, and Me-27/13-H, as well as the absence of NOE interactions between Me-27/Me-28, Me-27/9-H, 9-H/13-H, Me-28/5-H, and 13-H/15-H, were uniquely consistent with the stereochemistry of the C–B 6–6–5 tricyclic nucleus and the *Z* geometry for a double bond between C-14 and C-15. The results unambiguously establish compound **3** to be (13α*H*)-isomalabarica-14Z,17E,21-trien-3β-ol, a chair–boat 6–6–5 tricyclic product with *trans–syn–trans* stereochemistry and $\Delta^{14Z,17E,21}$ double bonds (Figure 1a). The second new product, migrating on the GC column with a retention time of 0.2 min relative to the first compound (i.e., **3**), was isolated and identified. The structure of compound **4** was also elucidated by NMR spectroscopy, as described in the Experimental Section. Interestingly, compound **4** is structurally similar to compound **3** with differences only in the stereochemistry of the carbon double bond located at the C-14/C-15 position. The presence of NOE interactions between Me-29/3-H, Me-29/5-H, Me-30/Me-28, Me-28/9-H, Me-27/13-H, and 13-H/15-H, as well as the absence of NOE interactions between Me-30/3-H, Me-28/Me-27, 13-H/9-H, 13-H/Me-26, and 15-H/Me-26, indicate the α-orientation for 13-H and the *E*-conformation for a double bond between C-14 and C-15. Thus, the structure was determined to be (13α*H*)-isomalabarica-14E,17E,21-trien-3β-ol (**4**), a tricyclic product with *trans–syn–trans* stereochemistry and $\Delta^{14E,17E,21}$ double bonds (Figure 1b). No known truncated or altered rearranged products, such as monocyclic achilleol A or camelliol C, bicyclic, tricyclic (13α*H*)-isomalabarica-14(26),17E,21-trien-3β-ol (**5**), tetracyclic protosta-20,24-dien-3β-ol, truncated rearranged protosta-12,24-dien-3β-ol, and altered deprotonated parkeol or 9β-lanosta-7,24-dien-3β-ol (Δ^7-lanosterol), were observed in the GC–MS analyses from any of the mutants. These two compounds, in conjunction with the previously isolated truncated tricyclic compound **5**, which abstracts the C-26 proton after generat-
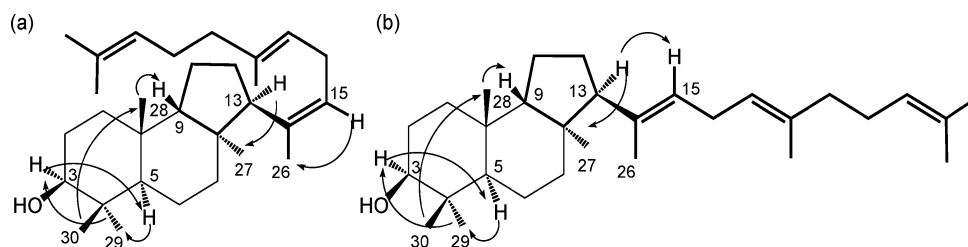
Figure 1. Bond connectivity and stereochemistry established by HMQC/HMBC (bold bond, —) and NOE interaction (curved arrows) of (a) (13αH)-isomalabarica-14Z,17E,21-trien-3β-ol and (b) (13αH)-isomalabarica14E, 17E,21-trien-3β-ol.

ing a tricyclic C-14 cation, suggested a direct trapping of the common C–B 6–6–5 tricyclic Markovnikov C-14 cation but with a different deprotonation position and stereochemistry.[16,17] Interestingly, Matsuda and co-workers characterized a baruol synthase (BARS1) from *Arabiopsis thaliana*, which makes baruol and 22 minor products.[22] Among the minor products, a tricyclic truncated product, (13S,14E,17E)-malabarica-14,17,21-trien-3β-ol, was isolated. However, no detailed structure–function relationships of baruol synthase were reported.

Amino acid substitution	Products profile		
	4	5	2
Gly	13	58	29
Ala	17	70	13
Val	0	0	100
Leu	0	0	100
Ile	17	33	50
Asp	8	5	87
Glu	0	44	56
Gln	0	0	100
Lys	0	0	100
Arg	0	0	100
Ser	13	69	18
Thr	21	59	20
Cys	0	0	100
Met	0	0	100
Phe	6	4	90
Trp	0	0	100
Pro	28	51	21
Asn	–	–	–
His	–	–	–

The production of truncated cyclization intermediates by ERG7[Y99X] mutants suggests that the substitution of Tyr99 effects the formation of truncated tricyclic triterpenes but does not result in loss of enforcement of the boat conformation for lanosterol B-ring formation. In ERG7[Y99X] mutants, the (13αH)-isomalabarica-trien-3β-ols 3 and 4 were apparently formed from intermediate C–B 6–6–5 Markovnikov tricyclic cation through deprotonation of C-15 (Scheme 1). Protonation of oxidosqualene initiates carbocation formation and subsequent cation–π annulation to a chair–boat–chair (C–B–C) conformation and Markovnikov-favored 6–6–5 tricyclic C-14 cation (III) without disruption at either

the monocyclic (I) or bicyclic (II) cationic position. In ERG7[H234X] and ERG7[F445X] site-saturated mutations, and ERG7[Y510F/H] site-directed mutations, direct deprotonation of Me-26 resulted in the formation of 5 as the truncated product, whereas in ERG7[Y99X] site-saturated mutations, deprotonation of different protons at the C-15 position produced compounds 3 and 4.[15,16,24] Alternatively, an anchimeric cyclopentylcarbinyl cyclohexyl carbocation (IV) rearrangement occurred between C-13 and C-14 and concertedly expanded the C-ring, which was followed by D-ring annulation to generate the protosteryl C-20 cation (V). Subsequently, a series of hydride and methyl group rearrangements generated the lanosteryl C-8/C-9 cation (VI). Finally, a highly specific deprotonation abstracted the proton, which was either originally at C-9 or, after the hydride shift from the C-9 to the C-8 position, and this deprotonation yields lanosterol.

The question of how the OSC catalyzes the course of C- and D-ring cyclization remains controversial.[5,15,16,25–27] Different mechanisms based on either experimental evidence or computational studies have been proposed for the formation of C- and D-ring intermediates. Formation of rings C and D could proceed by either the 6–6–5 Markovnikov tertiary cyclopentylcarbinyl carbocation (III), which undergoes an anchimeric cyclocarbinyl-cyclohexyl (IV) C-ring expansion and D-ring annulation, or the asynchronous concerted cyclization from A/B-bicyclic cyclohexyl cation (II) to D-ring formation to generate the protosteryl cation (V). However, many 6–6–5 tricycles occur in nature or arise from simple substrate analogs, whereas natural 6–6–6 triterpenes from (oxido)squalene are unknown, favorably supporting the intermediary of the 6–6–5 tertiary cyclopentylcarbinyl carbocation.[2,5,28–31] For example, Corey and co-workers performed substrate–analog experiments on *S. cerevisiae* ERG7 wild-type enzyme and obtained a discrete 6,6,5,4-tetracyclic compound involved in C-ring closure, providing convincing evidence for the 6–6–5 tertiary cyclopentylcarbinyl carbocation formation.[5] In addition, triterpenoid compounds with a 6–6–5 C–B tricyclic isomalabricane skeleton have been isolated from natural resources.[31] Furthermore, Hess showed that the cyclopentylcarbinyl carbocation formed during the lanosterol biosynthesis could quickly undergo a concerted C-ring expansion and D-ring closure to give the protosteryl cation without violation of the Markovnikov rule.[26] It was proposed that the OSC plays a functional role in "holding" the substrate in
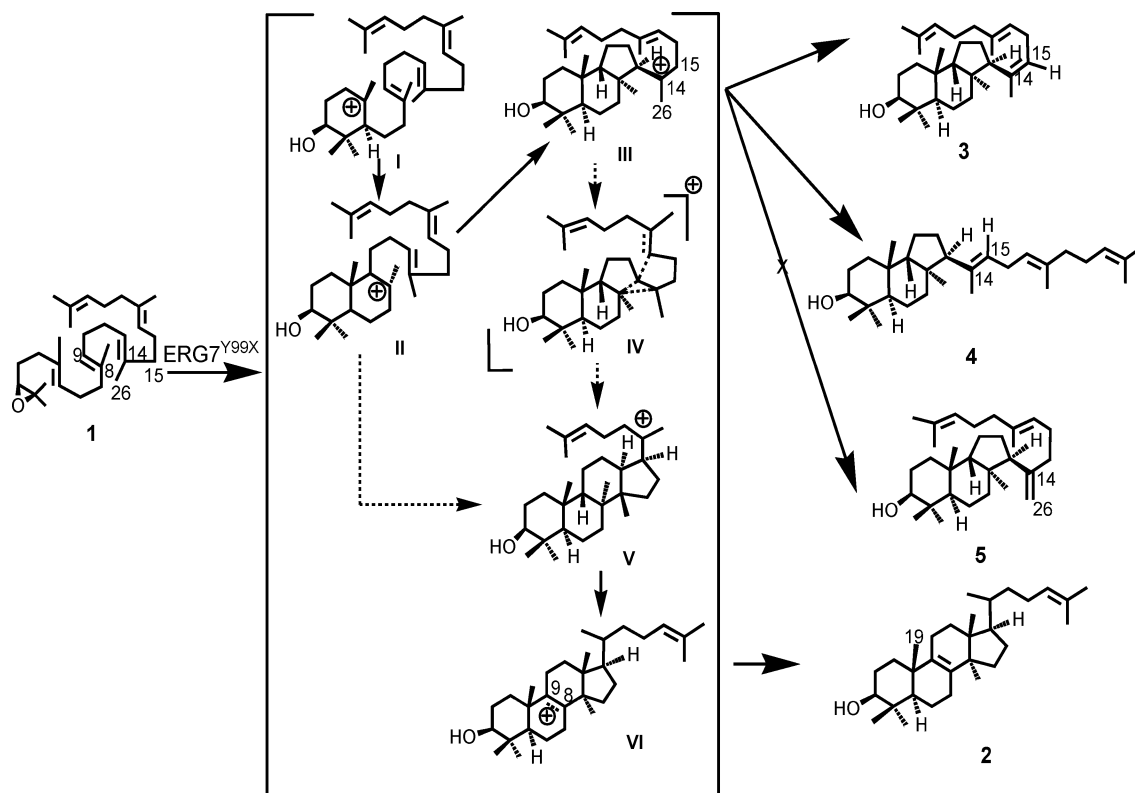
Scheme 1. Proposed mechanism for the oxidosqualene to lanosterol cyclization/rearrangement cascade in ERG7[Y99X]-catalyzed site-saturated mutants.

the proper conformation for the completion of the cascade leading to the tetracyclic system. We have previously isolated a Markovnikov 6–6–5 tricyclic intermediate from both the *S. cerevisiae* ERG7[H234X] and ERG7[F445X] mutants, which also supports the intermediary of the 6–6–5 tertiary cyclopentylcarbinyl carbocation for oxidosqualene cyclase-catalyzed cyclization reactions.[15,16] In contrast, a computational study of the squalene cyclase reaction performed by Ramkumar and Gao suggested that the only significant intermediate in the squalene-hopene cyclization cascade is the A/B-bicyclic cyclohexyl cation, and the six-membered C-ring species is not a minimum on the free energy surface whose formation is accompanied by an asynchronous concerted cyclization from the A/B-bicyclic cyclohexyl cation to ring D.[27] Nevertheless, the latter mechanism was only supported by the results obtained from free-energy simulation and the lack of isolation of a 6–6–6 tricyclic aborted cyclization product. However, it is interesting to note that following the B-ring formation, a branched free-energy profile for the C–B–C protosteryl cation and the C–C–C dammarenyl cation formation was observed. For the protosteryl cation, an endothermic 9.4 kcal/mol free energy relative to the bicyclic cation was obtained for the C–B 6–6–5 tricyclic cyclopentylcarbinyl cation. Conversely, for the dammarenyl cation formation, an exothermic 1.1 kcal/mol free energy relative to that of the C–C bicyclic cation was observed for the C–C–C 6–6–5 tricyclic cyclopentylcarbinyl cation. Subsequently, the protosteryl cation showed an endothermic 2.7 kcal/mol free energy relative to that of the 6–6–5 tricy-

clic cyclopentylcarbinyl carbocation, whereas the C–C–C 6–6–5 tricyclic cyclopentylcarbinyl cation exhibited an exothermic 6.9 kcal/mol of free energy relative to that of the dammarenyl cation. In parallel, Matsuda showed that a low-energy 6–6–5 pathway of C- and D-ring formation circumvents the 6–6–6 tricycle and that a horizontal variant of the secondary cyclohexyl carbocation occurs transiently as a partially bridged structure in D-ring formation, but is neither an intermediate nor transition state along the minimum-energy path.[30] Perhaps the low barrier of the free energy for the protosteryl cation formation could be compensated by the enzyme through "holding" of the proper carbocationic conformation, and the placement of the nucleophilic groups from the protein backbone or side chains and proceed through a concerted or bridged transition state in C-ring expansion/D-ring annulation to the protosteryl cation, as previously suggested by Jenson and Jorgenson and Hess.[25,26] Alternatively, we cannot exclude the possibility that stabilization or destabilization effects caused by the mutation may subsequently alter the C-ring cyclization process from asynchronous concerted A/B-bicyclic cyclohexyl carbocation to 6–6–5 Markovnikov tertiary cyclopentylcarbinyl-cyclohexyl rearrangements. However, a mutation in the enzyme active site may alter the conformation and positioning of the cyclizing polyolefin chain or disrupt specific interactions between the enzyme and the carbocationic intermediate that are needed for the delicate balance of thermodynamic or kinetic control of various carbocationic intermediates.

Why the ERG7^{Y99X} mutants exhibit different tricyclic deprotonation profiles from those of the ERG7^{H234X} and ERG7^{F445X} mutants is another interesting question. Both the ERG7^{H234X} and ERG7^{F445X} mutants yielded compound **5** as the sole tricyclic deprotonation product, whereas the ERG7^{Y99X} mutants resulted in the production of compounds **3** and **4**, but not **5** from the common C-14 cation. In addition, most of the ERG7^{Y99X} mutants produced 14(*Z*) isomer **3** as a major product. Previous results showed that progressive reaction energy release was primarily observed during A- and B-ring formation but was much less energetic for C- and D-ring annulation when neglecting the role of the enzyme. Nevertheless, the energetics of A-ring formation could be dramatically affected by the inclusion of the enzymatic effects.[30] In addition, comparing energies among various tricyclic geometric isomers showed energy decrements from compounds **5** to **3** to **4**, and although little influence on the enzymatic effect was observed when the tricyclic cation was converted into the tetracyclic intermediate, the substitution of amino acid residues at different spatial positions may alter a kinetically favored compound **5** that produces the thermodynamically favored compounds **3** and **4**. Perhaps, the differences in energies of various tricyclic geometric isomers could be compensated by the amino acid residues in the stabilization of the Markovnikov tricyclic cation and/or the subsequent alteration of the deprotonation position with differential stereochemical control, with compound **3** in favor of compound **4**. Further, the isolation of compounds **3** and **4**, but not that of compound **5**, suggested a discrepancy in the effects of spatially different amino acid residues within the active site cavity on both cationic stabilization and deprotonation.

In parallel, the homology modeling also provides some insight into the relationships between enzyme structure and product specificity (Figure 2). Residues in this region are involved in substrate folding, which affects the cyclization/rearrangement mechanism.[13] The homology model showed that His234 of ERG7 is hydrogen bonded to Tyr510 and located spatially near the upper back end of the active site cavity. The Phe445 residue of ERG7 is located near the B/C ring fusion and is proximal to the C-8 and C-14 positions, neighboring the ceiling of the active site cavity. Inspection of the model suggests that the Tyr99 residue is positioned in the middle side wall of the active site cavity by interacting with the C-ring, with the phenolic hydroxy side chain pointed towards the substrate. The C-14 cation was found at a distance of approximately 5.0 Å from the observed phenolic oxygen atom of Tyr99, and this distance agrees with the dipole–cation interaction for the phenolic oxygen atom of Tyr99 in the C-14 cation-bound OSC complex. It is conceivable that amino acid changes at Tyr99 would strongly affect the orientation or electrostatic interaction of the phenolic oxygen of Tyr99, which is positioned to stabilize the C-14 cation for C-ring expansion and further D-ring annulation. Perhaps some additional space for the free rotation of the hydrocarbon side chain moiety is offered through mutations at this position, resulting in protons being abstracted from different positions and/or orien-

tations. Alternatively, the possibility that mutations at Tyr99 generate a new base that leads to the Markovnikov C–B 6–6–5 cation and the subsequent disproportional formation of compounds **3** and **4** cannot be excluded. In contrast, a deletion at this position may lead to a local main chain adjustment in the mutant protein compared with the wild type, incurring obstruction of substrate binding and subsequent catalysis such that no product could be obtained from the ERG7$^{\Delta Y99}$ mutant.
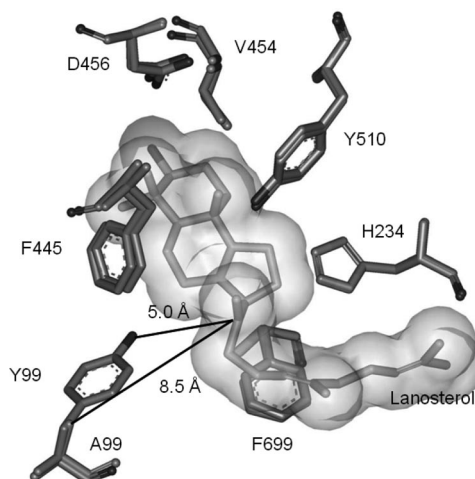
Figure 2. Snapshot of the superposition of the *S. cerevisiae* ERG7^{Y99} wild type structure with the ERG7^{Y99A} mutant structure, which corresponds to the tricyclic C-14 carbocation intermediate, which was obtained from homology modeling.

Conclusions

In conclusion, a genetic selection for active ERG7 mutant enzymes with substitutions at Tyr99, coupled with characterization of the products generated by those mutant enzymes, suggests that Tyr99 plays a role in catalysis, affecting both Markovnikov tricyclic C-14 cationic stabilization and the regio- or stereochemical control in the active site of the protons at the C-15 position for subsequent deprotonation but not the B-ring boat conformation. Characteristically, structural modification or electronic differentiation of active site residue substitutions or repositions may have effects on the stabilization of different cation intermediates or neighboring amino acid residues or motifs, thus directing truncated deprotonation from different orientations and subsequent stereochemical predilections. Moreover, inconsistencies were observed on the functional roles of human OSC structure-based prediction and *S. cerevisiae* ERG7 experimental results, suggesting that minor dissimilarities may occur between two enzymes and require independent characterization of their structure–function relationships. Finally, the results obtained from this study provide significant insight into the stereo- and regiocontrol of oxidosqualene cyclases in general. Further studies should focus on elucidating the precise molecular interactions in con-

trolling regio- and stereochemical specificity, chair–boat–chair and chair–chair–chair conformations, and the rearrangement process.

Experimental Section

Generation and Analysis of Mutant Extracts: The pTKERG7RSWT plasmid, a pRS314 derivative containing the *S. cerevisiae ERG7* gene, was used as a template for Y99 deletion and site-saturated mutagenesis. The following oligonucleotide primers used (with substitutions in bold and silent mutation italicized):

ERG7Y99X-Degenerate1:

5′-d(CCGTGTCAA**NNN**AAA*GGG*CCCATGTTCATG)-3′

ERG7Y99-Degenerate2:

5′-d(CATGAACAT*GGG*CCCTTT**NNN**TTGACACGG)-3′

ERG7Y99-Deletion1:

5′-d(CCGTGTCAAAAA*GGG*CCCATGTTCATG)-3′

ERG7Y99-Deletion2:

5′-d(CATGAACAT*GGG*CCCTTTTTGACACGG)-3′

The mutagenesis experiments were performed by using the QuikChange site-directed mutagenesis kit (Stratagene, La Jolla, CA).[15] Following confirmation of the mutations by DNA sequencing, recombinant plasmids were electroporated into the yeast strain TKW14 and selected for growth on SD+Ade+Lys+His+Met+Ura+hemin+G418+Erg plates (Calbiochem, La Jolla, CA, USA). The plasmids were then selected on SD+Ade+Lys+His+Met+Ura+hemin+G418+5-FOA plates for complementation of cyclase activity as described previously.[11,14] Transformants were grown in SD+Ade+Lys+His+Met+Ura+hemin+G418 +Erg medium for nonsaponifiable lipid (NSL) extraction and column chromatography. The NSL extract was fractionated by silica gel column chromatography and assayed by gas chromatography–mass spectrometry (GC–MS) to examine triterpenoid products with a molecular mass of *m/z* = 426. The mixture of **2**, **3**, and **4** (47–65 mg for different mutants, 1.4%–1.9% yield from the NSL extract) was obtained with n-hexane/ethyl acetate (19:1) as eluent. Relative ratios of each mutant were determined by the intensities of the signals in the GC–MS trace in conjunction with the resolved methyl peaks in the NMR spectrum, as described previously.[15]

Structure Characterization of (13α*H*)-Isomalabarica-14*Z*,17*E*,21-trien-3β-ol (3): The EI mass spectrum showed a molecular ion at *m/z* = 426 and fragment peaks at *m/z* = 357, 339, and 247, corresponding to $C_{30}H_{50}O$ [M]+, [M – C_5H_9]+, [M – C_5H_9 – H_2O]+, and [M – $C_{13}H_{21}$ – H_2]+, respectively, and suggesting a mass spectral fragmentation of incomplete cyclization. ¹H NMR spectroscopy showed distinct chemical shifts with four vinylic methyl signals (δ = 1.657, 1.600, 1.584, 1.577 ppm), four methyl singlets (δ = 1.072, 0.964, 0.918, 0.763 ppm), and three sets of triplet double bond protons (δ = 5.186, 5.076, 5.043 ppm). The HMQC spectrum showed that the olefinic protons at δ = 5.186, 5.076, and 5.043 ppm are attached to the carbon atoms at δ = 126.8 (C-15), 124.3 (C-21), and 123.3 (C-17) ppm, respectively, and that the methine proton at δ = 3.232 ppm is attached to the carbon atom at δ = 79.5 ppm (C-3). The HMQC spectrum also showed that the peak at δ = 2.585–2.627 ppm contained three protons, which are attached to carbon atoms at δ = 50.8 (C-13, 1 H) and 26.9 ppm (C-16, 2 H). The ¹³C NMR spectrum revealed the presence of three tertiary-quaternary substituted double bonds (δ = 123.3, 131.3 and 124.3, 134.8, as well

as 126.8, 137.8 ppm), which are characteristics of double bonds at the exocyclic hydrocarbon side chains. These correlations suggest the involvement of a tricyclic ring skeleton. The following are features of the HMBC spectrum: (1) The δ = 1.657 ppm protons of the methyl group are coupled by ²*J* to the carbon atom at δ = 131.3 ppm (C-22), as well as by ³*J* to the carbon atoms at δ = 124.3 (C-21) and 17.7 ppm (C-24), thus locating the terminal double bond. (2) The carbon atom at δ = 124.3 ppm is coupled to protons at δ = 2.038 and 1.967 ppm, as well as at δ = 1.657 and 1.577 ppm. (3) The carbon atom at δ = 123.3 ppm is coupled to protons at δ = 2.584–2.627, 1.967, 1.584, 5.186 ppm. and (4) The protons at δ = 2.584–2.627 ppm are coupled to carbon atoms at δ = 123.3 (C-17), 126.8 (C-15), 134.8 (C-18), and 137.8 ppm (C-14). These correlations unambiguously establish the connectivity of hydrocarbon side chains and relative double bond positions. Furthermore, the HMBC spectrum showed that the δ = 2.615 ppm methine proton is coupled by ²*J* to carbon atoms at δ = 137.8 (C-14), 44.2 (C-8), and 25.3 (C-12), as well as ³*J* to carbon atoms at δ = 126.8 (C-15), 54.4 (C-9), 21.2 (C-11), 22.2 (C-26), and 29.9 ppm (C-27), thus establishing the adjacent connectivity between the double bond and the tricyclic nucleus. Chemical shifts were referenced to $Si(CH_3)_4$ and are generally accurate to +0.01 ppm. ¹H NMR (600 MHz, CDCl₃): δ = 5.186 (t, *J* = 7.3 Hz, 1 H, 15-H), 5.043 (t, *J* = 7.6 Hz, 1 H, 17-H), 5.076 (t, *J* = 6.6 Hz, 1 H, 21-H), 3.237 (dd, *J* = 11.6, 5.1 Hz, 1 H, 3α-H), 2.585–2.627 (m, 2 H for 16-H, 1 H for 13α-H), 2.045 (m, 2 H, 20-H), 1.960 (m, 2 H, 19-H), 1.860 (m, 1 H, 12α-H), 1.708–1.786 (m, 3 H, 2α-H, 7-H), 1.657 (s, 3 H, 23-H), 1.626 (m, 1 H, 2β-H), 1.600 (s, 3 H, 26-H), 1.584 (s, 3 H, 25-H), 1.577 (s, 3 H, 24-H), 1.563 (m, 2 H, 9β-H, 11β-H), 1.547 (m, 1 H, 12β-H), 1.532 (m, 1 H, 6α-H), 1.507 (m, 1 H, 6β-H), 1.485 (m, 1 H, 5α-H), 1.457 (m, 1 H, 1β-H), 1.450 (m, 1 H, 11β-H), 1.389 (m, 1 H, 1α-H), 1.239 (m, 1 H, 6β-H), 1.072 (s, 3 H, 27-H), 0.964 (s, 3 H, 29-H), 0.918 (s, 3 H, 28-H), 0.763 (s, 3 H, 30-H) ppm. ¹³C NMR (150 MHz, CDCl₃): δ = 33.8 (C-1), 29.2 (C-2), 79.5 (C-3), 39.1 (C-4), 47.6 (C-5), 18.8 (C-6), 32.5 (C-7), 44.2 (C-8), 54.4 (C-9), 35.6 (C-10), 21.2 (C-11), 25.3 (C-12), 50.8 (C-13), 137.8 (C-14), 126.8 (C-15), 26.9 (C-16), 123.3 (C-17), 134.8 (C-18), 39.7 (C-19), 26.7 (C-20), 124.3 (C-21), 131.3 (C-22), 17.7 (C-23), 25.7 (C-24), 16.1 (C-25), 22.2 (C-26), 29.9 (C-27), 23.1 (C-28), 29.1 (C-29), 15.9 (C-30) ppm.

Structure Characterization of (13α*H*)-Isomalabarica-14*E*,17*E*,21-trien-3β-ol (4): The EI low-resolution mass spectrum exhibited similar parent peak and fragment peak patterns to compound **3**, suggesting an analogous nucleus skeleton of incomplete cyclization. The ¹H NMR spectrum showed four distinct vinylic methyl signals (δ = 1.662, 1.605, 1.582, 1.551 ppm), four methyl singlets (δ = 1.044, 0.956, 0.912, 0.756 ppm), and three double bond protons (δ = 4.997, 5.081, 5.094 ppm), suggesting a tricyclic ring skeleton. Next, a combination of the apparent HMQC and HMBC correlations showed the following features: (1) The vinyl proton at δ = 4.997 ppm (δ_C = 125.0 ppm, C-15) is coupled to carbon atoms at 27.0 (C-16), 123.3 (C-17), 59.5 (C-13), and 18.1 ppm (C-26). (2) The vinyl proton at δ = 5.094 ppm (δ_C = 123.3 ppm, C-17) is coupled to carbon atoms at δ = 27.0 (C-16), 39.7 (C-19), and 16.1 ppm (C-25). (3) The vinyl proton at δ = 5.081 ppm (δ_C = 124.32 ppm, C-21) is coupled to carbon atoms at δ = 25.7 (C-23) and 17.7 ppm (C-24). (4) The proton at δ = 2.684 ppm (δ_C = 27.0 ppm, C-16) is coupled to carbon atoms at δ = 139.2 (C-14), 125.0 (C-15), 123.3 (C-17), and 135.0 ppm (C-18). (5) The proton at δ = 2.048 ppm (δ_C = 59.5 ppm, C-13) is coupled to carbon atoms at δ = 139.2 (C-14), 125.0 (C-15), 44.5 (C-8), 52.9 (C-9), and 29.8 ppm (C-27). These correlations unequivocally established the bond connectivity between the tricyclic nucleus skeleton and the

exocyclic hydrocarbon side chain, as well as the double bond positions. Chemical shifts were referenced to $Si(CH_3)_4$ and are generally accurate to +0.01 ppm. ^{1}H NMR (600 MHz, CDCl$_3$): δ = 5.094 (t, J = 7.1 Hz, 1 H, 17-H), 5.069 (t, J = 7.3 Hz, 1 H, 21-H), 4.997 (t, J = 7.0 Hz, 1 H, 15-H), 3.231 (dd, J = 11.7, 5.0 Hz, 1 H, 3α-H), 2.687 (m, 2 H, 16-H), 2.078–2.047 (m, 3 H, 2 H for 20-H, 1 H for 13α-H), 1.964 (m, 2 H, 19-H), 1.874–1.928 (m, 1 H, 12α-H), 1.711–1.739 (m, 1 H, 2α-H), 1.662 (s, 3 H, 23-H), 1.622 (m, 2 H, 1 H for 2β-H, 1 H for 7α-H), 1.605 (s, 3 H, 25-H), 1.582 (s, 3 H, 24-H), 1.551 (s, 3 H, 26-H), 1.537–1.511 (m, 4 H, 1 H for 6α-H, 1 H for 9β-H, 1 H for 11β-H, 1 H for 12β-H), 1.470–1.420 (m, 1 H, 5α-H), 1.387 (m, 3 H, 2 H for 1-H, 1 H for 11α-H), 1.222–1.202 (m, 2 H, 1 H for 6β-H, 1 H for 7β-H), 1.044 (s, 3 H, 27-H), 0.956 (s, 3 H, 29-H), 0.911 (s, 3 H, 28-H), 0.756 (s, 3 H, 30-H) ppm. ^{13}C NMR (150 MHz, CDCl$_3$): δ = 34.1 (C-1), 29.1 (C-2), 79.5 (C-3), 39.0 (C-4), 47.0 (C-5), 18.6 (C-6), 32.1 (C-7), 44.5 (C-8), 52.9 (C-9), 35.4 (C-10), 20.9 (C-11), 26.9 (C-12), 59.5 (C-13), 139.2 (C-14), 125.0 (C-15), 27.0 (C-16), 123.3 (C-17), 135.0 (C-18), 39.7 (C-19), 26.7 (C-20), 124.3 (C-21), 131.3 (C-22), 25.7 (C-23), 17.7 (C-24), 16.1 (C-25), 18.1 (C-26), 29.8 (C-27), 23.1 (C-28), 29.1 (C-29), 15.9 (C-30) ppm.

Supporting Information (see footnote on the first page of this article): MS, ^{1}H NMR, ^{13}C NMR, HMQC, HMBC spectra of compounds **3** and **4**.

Acknowledgments

[1] I. Abe, M. Rohmer, G. D. Prestwich, *Chem. Rev.* **1993**, *93*, 2189–2206.

[2] K. U. Wendt, G. E. Schulz, E. J. Corey, D. R. Liu, *Angew. Chem. Int. Ed.* **2000**, *39*, 2812–2833.

[3] E. J. Corey, H. Cheng, C. H. Baker, S. P. T. Matsuda, D. Li, X. Song, *J. Am. Chem. Soc.* **1997**, *119*, 1289–1296.

[4] E. J. Corey, S. C. Virgil, *J. Am. Chem. Soc.* **1991**, *113*, 4025–4026.

[5] E. J. Corey, S. C. Virgil, H. Cheng, C. H. Baker, S. P. T. Matsuda, V. Singh, S. Sarahar, *J. Am. Chem. Soc.* **1995**, *117*, 11819–11820.

[6] K. U. Wendt, K. Poralla, G. E. Schulz, *Science* **1997**, *277*, 1811–1815.

[7] E. A. Hart, L. Hua, L. B. Darr, W. K. Wilson, J. Pang, S. P. T. Matsuda, *J. Am. Chem. Soc.* **1999**, *121*, 9887–9888.

[8] B. M. Joubert, L. Hua, S. P. T. Matsuda, *Org. Lett.* **2000**, *2*, 339–341.

[9] S. Lodeiro, M. J. Segura, M. Stahl, T. Schulz-Gasch, S. P. T. Matsuda, *ChemBioChem* **2004**, *5*, 1581–1585.

[10] M. M. Meyer, M. J. Segura, W. K. Wilson, S. P. T. Matsuda, *Angew. Chem. Int. Ed.* **2000**, *39*, 4090–4092.

[11] T. K. Wu, J. H. Griffin, *Biochemistry* **2002**, *41*, 8238–8244.

[12] T. K. Wu, C. H. Chang, *ChemBioChem* **2004**, *5*, 1712–1715.

[13] R. Thoma, T. Schulz-Gasch, B. D'Arcy, J. Benz, J. Aebi, H. Dehmlow, M. Henning, M. Stihle, A. Ruf, *Nature* **2004**, *432*, 118–122.

[14] T. K. Wu, Y. T. Liu, C. H. Chang, *ChemBioChem* **2005**, *6*, 1177–1181.

[15] T. K. Wu, Y. T. Liu, C. H. Chang, M. T. Yu, H. J. Wang, *J. Am. Chem. Soc.* **2006**, *128*, 6414–6419.

[16] T. K. Wu, Y. T. Liu, F. H. Chiu, C. H. Chang, *Org. Lett.* **2006**, *8*, 4691–4694.

[17] T. K. Wu, M. T. Yu, Y. T. Liu, C. H. Chang, H. J. Wang, E. W. G. Diau, *Org. Lett.* **2006**, *8*, 1319–1322.

[18] T. K. Wu, C. H. Chang, Y. T. Liu, T. T. Wang, *Chem. Rec.* **2008**, *8*, 302–325.

[19] T. K. Wu, H. Y. Wen, C. H. Chang, Y. T. Liu, *Org. Lett.* **2008**, *10*, 2529–2532.

[20] T. K. Wu, T. T. Wang, C. H. Chang, Y. T. Liu, *Org. Lett.* **2008**, *10*, 4959–4962.

[21] T. Schulz-Gasch, M. Stahl, *J. Comput. Chem.* **2003**, *24*, 741–753.

[22] S. Lodeiro, Q. Xiong, W. K. Wilson, M. D. Kolesnikova, C. S. Onak, S. P. T. Matsuda, *J. Am. Chem. Soc.* **2007**, *129*, 11213–11222.

[23] The in vivo TKW14[pERG7Y99X] product profiles represent metabolic equilibrium of lanosterol and related triterpenes under physiological conditions, which may vary from that of the in vitro assay.

[24] S. Lodeiro, W. K. Wilson, H. Shan, S. P. T. Matsuda, *Org. Lett.* **2006**, *8*, 439–442.

[25] C. Jenson, W. L. Jorgenson, *J. Am. Chem. Soc.* **1997**, *119*, 10846–10854.

[26] B. A. Hess Jr, *J. Am. Chem. Soc.* **2002**, *124*, 10286–10287.

[27] R. Rajamani, J. Gao, *J. Am. Chem. Soc.* **2003**, *125*, 12768–12781.

[28] T. Hoshino, M. Kouda, T. Abe, S. Ohashi, *Biosci. Biotechnol. Biochem.* **1999**, *63*, 2038–2041.

[29] R. Xu, G. C. Fazio, S. P. T. Matsuda, *Phytochemistry* **2004**, *65*, 261–291.

[30] S. P. T. Matsuda, W. K. Wilson, Q. Xiong, *Org. Biomol. Chem.* **2006**, *4*, 530–543.

[31] L. McCabe, J. Clardy, *Tetrahedron Lett.* **1982**, *23*, 3307–3310.